

7<sup>TH</sup>  
EDITION

# THE FINITE ELEMENT METHOD FOR FLUID DYNAMICS



O.C. Zienkiewicz, R.L. Taylor & P. Nithiarasu



# The Finite Element Method for Fluid Dynamics

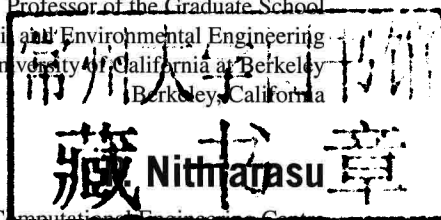
## Seventh Edition

**O.C. Zienkiewicz, CBE, FRS**

Previously UNESCO Professor of Numerical Methods in Engineering  
International Centre for Numerical Methods in Engineering, Barcelona  
Previously Director of the Institute for Numerical Methods in Engineering  
University of Wales, Swansea

**R.L. Taylor**

Professor of the Graduate School  
Department of Civil and Environmental Engineering  
University of California at Berkeley  
Berkeley, California



Civil and Computational Engineering Centre  
School of Engineering, Swansea University



AMSTERDAM • BOSTON • HEIDELBERG • LONDON  
NEW YORK • OXFORD • PARIS • SAN DIEGO  
SAN FRANCISCO • SINGAPORE • SYDNEY • TOKYO

Butterworth-Heinemann is an imprint of Elsevier



Butterworth-Heinemann is an imprint of Elsevier  
The Boulevard, Langford Lane, Kidlington, Oxford, OX5 1GB  
225 Wyman Street, Waltham, MA 02451, USA

First published 1967 by McGraw-Hill

Fifth edition published by Butterworth-Heinemann 2000

Reprinted 2002

Sixth edition 2005

Reprinted 2006

Seventh edition 2014

Copyright © 2014, 2005, 2000 Elsevier Ltd. All rights reserved

No part of this publication may be reproduced or transmitted in any form or by any means, electronic or mechanical, including photocopying, recording, or any information storage and retrieval system, without permission in writing from the publisher. Details on how to seek permission, further information about the Publisher's permissions policies and our arrangement with organizations such as the Copyright Clearance Center and the Copyright Licensing Agency, can be found at our website: [www.elsevier.com/permissions](http://www.elsevier.com/permissions).

This book and the individual contributions contained in it are protected under copyright by the Publisher (other than as may be noted herein).

#### **Notices**

Knowledge and best practice in this field are constantly changing. As new research and experience broaden our understanding, changes in research methods, professional practices, or medical treatment may become necessary.

Practitioners and researchers must always rely on their own experience and knowledge in evaluating and using any information, methods, compounds, or experiments described herein. In using such information or methods they should be mindful of their own safety and the safety of others, including parties for whom they have a professional responsibility.

To the fullest extent of the law, neither the Publisher nor the authors, contributors, or editors, assume any liability for any injury and/or damage to persons or property as a matter of products liability, negligence or otherwise, or from any use or operation of any methods, products, instructions, or ideas contained in the material herein.

#### **British Library Cataloguing in Publication Data**

A catalogue record for this book is available from the British Library

#### **Library of Congress Cataloguing in Publication Data**

A catalog record for this book is available from the Library of Congress

ISBN: 978-1-85617-635-4

For information on all Butterworth-Heinemann publications  
visit our website at [store.elsevier.com](http://store.elsevier.com)

Printed and bound in the United States

14 15 16 17 10 9 8 7 6 5 4 3 2 1



Working together  
to grow libraries in  
developing countries

[www.elsevier.com](http://www.elsevier.com) • [www.bookaid.org](http://www.bookaid.org)

# The Finite Element Method for Fluid Dynamics

**Professor O.C. Zienkiewicz**, CBE, FRS, FREng died on January 2, 2009. Prior to his death he was Professor Emeritus at the Civil and Computational Engineering Centre, University of Wales, Swansea and previously was Director of the Institute for Numerical Methods in Engineering at the University of Wales, Swansea, UK. He also held the UNESCO Chair of Numerical Methods in Engineering at the Technical University of Catalunya, Barcelona, Spain. He was the head of the Civil Engineering Department at the University of Wales, Swansea between 1961 and 1989. During this period he established that department as one of the primary centers of finite element research. In 1968 he became the Founder Editor of the *International Journal for Numerical Methods in Engineering* which still remains today the major journal in this field. The recipient of 27 honorary degrees and many medals, he was a member of five academies—an honor he received for his many contributions to the fundamental developments of the finite element method. In 1978, Professor Zienkiewicz became a Fellow of the Royal Society and the Royal Academy of Engineering. This was followed by his election as a foreign member to the US Academy of Engineering (1981), the Polish Academy of Science (1985), the Chinese Academy of Sciences (1998), and the National Academy of Science, Italy (Accademia dei Lincei) (1999). He published the first edition of this book in 1967 and it remained the only book on the subject until 1971.

**Professor R.L. Taylor** has more than 50 years' experience in the modeling and simulation of structures and solid continua including 8 years in industry. He is Professor of the Graduate School and the Emeritus T.Y. and Margaret Lin Professor of Engineering at the University of California at Berkeley and also Corporate Fellow at Dassault Systèmes SIMULIA in Providence, Rhode Island. In 1991 he was elected to membership in the US National Academy of Engineering in recognition of his educational and research contributions to the field of computational mechanics. He is a Fellow of the US Association of Computational Mechanics—USACM (1996) and a Fellow of the International Association of Computational Mechanics—IACM (1998). He has received numerous awards including the Berkeley Citation, the highest honor awarded by the University of California at Berkeley, the USACM John von Neumann Medal, the IACM Gauss-Newton Congress Medal, and a Dr.-Ingenieur ehrenhalber awarded by the Technical University of Hannover, Germany. He has written several computer programs for finite element analysis of structural and nonstructural systems, one of which, *FEAP*, is used worldwide in education and research environments. A personal version, *FEAPpv*, available at his UC website, is incorporated into this book.

**Professor P. Nithiarasu** has over 20 years' experience in finite element-based computational fluid dynamics research. He moved to Swansea in 1996 after completing his PhD research at IIT Madras and is currently Professor in the Civil and Computational Engineering Centre at Swansea University. He was awarded the Zienkiewicz silver medal and prize of the Institution of Civil Engineers, UK in 2002. In 2004 he was selected to receive the European Community on Computational Methods in Applied Sciences (ECCOMAS) award for young scientists in computational engineering sciences. He is the author of nearly 300 articles in the area of fluid dynamics, porous medium flows, and the finite element method. He is the founding editor of the *International Journal for Numerical methods in Biomedical Engineering*.

*This book is dedicated to the memory of  
Olgierd C. (Olek) Zienkiewicz:  
Pioneer, mentor, and close friend.*

# List of Figures

1.1	Coordinate direction and the infinitesimal control volume.	8
1.2	Basis function in linear polynomials for a patch of triangular elements.	18
1.3	(a) Three-node triangular element and (b) shape function for $N_1$ .	19
1.4	Linear triangular elements for Poisson equation example: (a) "connected" equations for node 1; (b) Type 1 and Type 2 element shapes in mesh.	21
1.5	Potential flow solution around an aerofoil. Mesh and streamline plots.	24
1.6	Free surface potential flow, illustrating an axisymmetric jet impinging on a hemispherical thrust reverser (from Sarpkaya and Hiriart [20]).	25
1.7	Finite volume weighting. Vertex centered method.	26
1.8	Finite volume domain and integrations for vertex centered method: "connected" equations for node 1; (b) Type 1 and Type 2 element boundary integrals.	27
2.1	A linear shape function for a one-dimensional problem.	35
2.2	Approximations to $Ud\phi/dx - kd^2\phi/dx^2 = 0$ for $\phi(0) = 1$ and $\phi(L) = 0$ for various Peclet numbers. Solid line: exact solution; dotted line with triangular symbol: standard Galerkin solution.	36
2.3	Approximations to $Ud\phi/dx - kd^2\phi/dx^2 = 0$ for $\phi = 0$ at $x = 0$ and $\phi = 1$ at $x = L$ for various Peclet numbers.	38
2.4	Petrov-Galerkin weight function $W_a = N_a + \alpha W_a^*$ . Continuous and discontinuous definitions.	39
2.5	Critical (stable) and optimal values of the "upwind" parameter $\alpha$ for different values of $Pe = Uh/2k$ .	40
2.6	Application of standard Galerkin and Petrov-Galerkin (optimal) approximation: (a) variable source term equation with constants $k$ and $h$ ; (b) variable source term with a variable $U$ .	41
2.7	A one-dimensional pure convective problem ( $k = 0$ ) with a variable source term $Q$ and constant $U$ . The Petrov-Galerkin procedure results in an exact solution but simple finite difference upwinding gives substantial error.	42
2.8	Assembly of one-dimensional quadratic elements.	48

2.9	A two-dimensional, streamline assembly. Element size $h$ and streamline directions.	50
2.10	"Streamline" procedures in a two-dimensional problem of pure convection. Bilinear elements [35]: (a) boundary conditions for test problem; solutions for $\theta = 45^\circ$ (top) and $\theta = 65^\circ$ .	52
2.11	The wave nature of a solution with no conduction. Constant wave velocity $U$ .	55
2.12	Mesh updating and interpolation: (a) forward and (b) backward.	58
2.13	Distortion of convected shape function.	60
2.14	A simple characteristic-Galerkin procedure.	60
2.15	Stability limit for lumped mass approximation and optimal upwind parameter.	65
2.16	Advection of a Gaussian cone in a rotating fluid by characteristic-Galerkin method: (a) original form; (b) form after one revolution using consistent $\mathbf{M}$ matrix; and (c) form after one revolution using lumped mass (Lax-Wendroff).	67
2.17	Characteristic-Galerkin method in the solution of a one-dimensional wave progression. Effect of using a lumped mass matrix and one of consistent iteration: (a) Courant number = 0.5; (b) Courant number = 0.1.	68
2.18	A Gaussian distribution advected in a constant velocity field. Boundary condition causes no reflection.	69
2.19	Progression of a wave with velocity $U = \phi$ .	72
2.20	Development of a shock (Burger equation): (a) profile at time $t = 0$ ; (b) characteristics; (c) profile at time $t = 1$ ; (d) profile at time $t = 2$ .	73
2.21	Propagation of a steep wave by Taylor-Galerkin process: (a) explicit methods $C = 0.5$ , step wave at $Pe = 12,500$ and (b) explicit methods $C = 0.1$ , step wave at $Pe = 12,500$ .	75
2.22	Propagation of a steep front in Burger's equation with solution obtained using different values of $C_{Lap}$ .	76
2.23	Solution of pure convection in element-by-element manner. Source term $Q$ and constant $u$ : (a) one-dimensional solution sequence; (b) two-dimensional solution sequence.	77
2.24	Solution of one-dimensional convection-diffusion problem: (a) one-dimensional linear element solution; (b) one-dimensional quadratic element solution.	79
3.1	Element sizes at different nodes of a linear triangle.	102
3.2	Fictitious and real boundaries.	111



3.3	Inviscid flow past a NACA0012 aerofoil $\alpha = 0$ : (a) unstructured mesh with 1824 elements and 969 nodes; (b) details of mesh near stagnation point; (c) steady-state convergence for $M = 0.5$ with two- and single-step schemes, fully explicit form; (d) steady-state convergence for $M = 1.2$ for two-step scheme; (e) steady-state convergence for $M = 1.2$ for single-step scheme.	114
3.4	Subsonic inviscid flow past a NACA0012 aerofoil with $\alpha = 0$ and $M = 0.5$ : (a) density contours with TG scheme with no additional viscosity; (b) density contours with TG scheme with additional viscosity; (c) density contours with CBS scheme with no additional viscosity; (d) comparison of density along the stagnation line.	115
3.5	Vortex decay. Temporal convergence of the dual time-stepping quasi-implicit scheme with first-, second-, and third-order backward difference formula for $\Delta u^n / \Delta \tau$ : (a) velocity; (b) pressure.	117
4.1	Incompressible flow in a lid-driven cavity. Geometry and meshes. (a) Geometry and boundary conditions; (b) nonuniform structured mesh (elements: 2888, nodes: 1521); (c) uniform structured mesh (elements: 20,000, nodes: 10,201); (d) nonuniform unstructured mesh (elements: 10,596, nodes: 5515).	130
4.2	Incompressible flow in a lid-driven cavity: (a) $Re = 100$ , stream traces; (b) $Re = 100$ , pressure contours; (c) $Re = 400$ , stream traces; (d) $Re = 400$ , pressure contours.	131
4.3	Incompressible flow in a lid-driven cavity: (a) $Re = 5000$ , stream traces on the unstructured mesh; (b) $Re = 5000$ , stream traces on the uniform structured mesh; (c) $Re = 5000$ , pressure contours on the unstructured mesh; (d) $Re = 5000$ , pressure contours on the uniform structured mesh.	132
4.4	Incompressible flow in a lid-driven cavity. Horizontal velocity distribution at different Reynolds numbers: (a) $Re = 0$ ; (b) $Re = 400$ ; (c) $Re = 1000$ ; (d) $Re = 5000$ .	133
4.5	Incompressible flow in a lid-driven cavity. Vertical velocity distribution at different Reynolds numbers: (a) $Re = 0$ ; (b) $Re = 400$ ; (c) $Re = 1000$ ; (d) $Re = 5000$ .	134
4.6	Incompressible flow in a 3D lid-driven cavity. Mesh and contours at $Re = 400$ : (a) unstructured mesh; (b) $u_1$ contours; (c) $u_3$ contours; (d) pressure contours.	135
4.7	Lid-driven cavity. Steady-state convergence histories for (a) $Re = 400$ and (b) 5000. Comparison between fully explicit and semi-implicit schemes.	136
4.8	Incompressible flow past a backward facing step. Geometry and boundary conditions.	136
4.9	Incompressible flow past a backward facing step. step: (a) unstructured mesh; (b) $u_1$ velocity contours; (c) pressure contours ( $Re = 229$ ).	136

4.10	Incompressible flow past a backward facing step. Comparison between experimental [10] and numerical data, $Re = 229$ .	137
4.11	Incompressible flow past a sphere: (a) unstructured mesh; (b) unstructured mesh, cross section.	138
4.12	Incompressible flow past a sphere: (a) $u_1$ contours, $Re = 100$ ; (b) pressure contours, $Re = 100$ ; (c) $u_1$ contours, $Re = 200$ ; pressure contours, $Re = 200$ .	139
4.13	Incompressible flow past a sphere. Coefficient of pressure distribution on the surface along the flow direction [15–17]: (a) $Re = 100$ ; (b) $Re = 200$ .	140
4.14	Transient flow past a circular cylinder, $Re = 100$ : (a) unstructured mesh; (b) vertical velocity fluctuation at the exit mid-point; (c) drag history.	141
4.15	Lid-driven cavity. Horizontal and vertical velocity distributions along the centerline cross-sections, $Re = 1000$ .	142
4.16	Interpolation error in a one-dimensional problem with linear shape functions.	144
4.17	Element elongation $\delta$ and minimum and maximum element sizes.	147
4.18	Lid-driven cavity, $Re = 5000$ . Adapted meshes using curvature- and gradient-based refinements and solutions: (a) curvature-based procedure (nodes: 2389, elements: 4599); (b) gradient-based procedure (nodes: 1034, elements: 1962); (c) comparison of velocity at mid-vertical plane.	150
4.19	Transient incompressible flow around a cylinder at $Re = 250$ . Adaptively refined mesh. Pressure contours and streamlines at various times after initiation of “vortex shedding”: (a) $t = 6$ s; (b) $t = 11.5$ s; (c) $t = 16.5$ s.	152
4.20	Some useful velocity-pressure interpolations and their asymptotic, energy norm convergence rates: (a) continuous $p$ interpolation; (b) discontinuous $p$ interpolation.	154
5.1	Stress $\bar{\sigma}$ , viscosity $\mu$ , and strain rate $\dot{\epsilon}$ relationships for various materials: (a) linear, Newtonian, fluid; (b) non-Newtonian polymers; (c) viscoplastic-plastic metals.	164
5.2	Forming processes typically used in manufacture: (a) steady rate; (b) transient	166
5.3	Plane strain extrusion (extrusion ratio 2:1) with ideal plasticity assumed.	168
5.4	Steady-state rolling process with thermal coupling [40]: (a) geometry; (b) velocity profiles; (c) temperature distribution for different entry temperatures.	170
5.5	Punch indentation problem (penalty function approach) [4]. Updated mesh and surface profile with 24 isoparametric elements. Ideally plastic material; (a), (b), (c), and (d) show various depths of indentation (reduced integration is used here).	171

5.6	(a) A material grid and updated and adapted meshes with material deformation ( $\eta$ percentage in energy norm). A transient extrusion problem with temperature and strain-dependent yield [42]. Adaptive mesh refinement uses T6/1D elements of Fig. 4.20 (b) Contours of state parameters at $t = 2.9$ s; (c) load versus time.	172
5.7	Deep drawing by a flat-nosed punch [50].	175
5.8	Finite element simulation of the superplastic forming of a thin sheet component by air pressure application. This example considers the superplastic forming of a truncated ellipsoid with a spherical indent. The original flat blank was $150 \times 100$ mm. The truncated ellipsoid is 20 mm deep. The original thickness was 1 mm. The minimum final thickness was 0.53 mm; 69 time steps were used with a total of 285 Newton-Raphson iterations (complete equation solutions) [53]: (a) mesh of 856 elements for sheet idealization; (b) mesh for establishing die geometry; (c) deformed sheets at various times.	176
5.9	Physical representation of Maxwell model using spring and dashpot.	178
5.10	Physical representation of Oldroyd-B model using spring and dashpots.	178
5.11	Viscoelastic flow past a circular cylinder. Geometry and boundary conditions.	181
5.12	Viscoelastic flow past a circular cylinder. Unstructured mesh (nodes: 10,619; elements: 20,384) (a) mesh; (b) mesh in the vicinity of the cylinder.	183
5.13	Stokes flow past a circular cylinder. $Re = 0$ , $De = 0.0$ . Contours of velocity components and pressure: (a) $u_1$ velocity contours, $u_{1\min} = 0$ , $u_{1\max} = 2.94$ ; (b) $u_2$ velocity contours, $u_{2\min} = -0.895$ , $u_{2\max} = 0.893$ ; (c) pressure contours, $p_{\min} = -29.28$ , $p_{\max} = 36.04$ .	183
5.14	Viscoelastic flow past a circular cylinder. $Re = 0$ , $De = 0.5$ . Contours of velocity, pressure, and elastic stresses: (a) $u_1$ velocity contours, $u_{1\min} = 0$ , $u_{1\max} = 2.99$ ; (b) $u_2$ velocity contours, $u_{2\min} = -0.929$ , $u_{2\max} = 0.884$ ; (c) pressure contours, $p_{\min} = -28.35$ , $p_{\max} = 34.97$ ; (d) $\tau_{11}^V$ contours, $\tau_{11\min}^V = -0.979$ , $\tau_{11\max}^V = 76.45$ ; (e) $\tau_{12}^V$ contours, $\tau_{12\min}^V = -18.59$ , $\tau_{12\max}^V = 22.92$ ; (f) $\tau_{22}^V$ contours, $\tau_{22\min}^V = -0.463$ , $\tau_{22\max}^V = 16.82$ .	184
5.15	Viscoelastic flow past a circular cylinder. Comparison of drag force distribution with other available numerical data. Dou and Phan-Thian1 = Plain Oldroyd-B formulation without stress splitting; Dou and Phan-Thian2 = EVSS; Dou and Phan-Thian3 = DEVSS- $\omega$ ; Dou and Phan-Thian4 = DAVSS- $\omega$ ; Dou and Phan-Thian5 = Extrapolated results for zero mesh size.	185

5.16	Axisymmetric solutions to the bar impact problem: (a) initial shape; (b) linear triangles—displacement algorithm; (c) bilinear quadrilaterals—displacement algorithm; (d) linear triangles—CBS algorithm; (e) bilinear quadrilaterals—CBS algorithm.	186
5.17	Three-dimensional solution: (a) tetrahedral elements—standard displacement algorithm; (b) tetrahedral elements—CBS algorithm.	187
6.1	Typical problems with a free surface.	196
6.2	Broken dam problem. Problem definition and schematic of the free surface.	198
6.3	Broken dam problem. Mesh and contours after $t = 2.0$ : (a) mesh; (b) $u_1$ velocity contours; (c) $u_2$ velocity contours; (d) pressure contours.	199
6.4	Broken dam problem. Mesh and contours after $t = 5.0$ : (a) mesh; (b) $u_1$ velocity contours; (c) $u_2$ velocity contours; (d) pressure contours.	200
6.5	Broken dam problem. Comparison of numerical results with experimental data [45].	200
6.6	A typical problem of ship motion.	201
6.7	A submerged hydrofoil. Mesh updating procedure. Euler flow. Mesh after 1900 iterations.	204
6.8	A submerged hydrofoil. Mesh updating procedure. Euler flow: (a) pressure distribution; (b) comparison with experiment.	205
6.9	A submerged hydrofoil. Hydrostatic adjustment. Euler flow: (a) pressure contours and surface wave pattern; (b) comparison with experiment [68].	206
6.10	A submerged hydrofoil. Hydrostatic adjustment. Navier-Stokes flow: (a)–(d) magnitude of total velocity contours for different Reynolds numbers; (e) wave profiles for different Reynolds numbers.	207
6.11	Submerged DARPA submarine model: (a) surface mesh; (b) wave pattern.	208
6.12	A sailing boat: (a) surface mesh of hull, keel, bulb, and rudder; (b) wave profile.	209
6.13	ALE description in Cartesian coordinates.	210
6.14	Solitary wave propagation. Problem definition.	212
6.15	Solitary wave propagation. Meshes at various time levels: (a) $t = 0.0$ ; (b) $t = 2.28$ ; (c) $t = 4.58$ , (d) $t = 6.84$ ; (e) $t = 9.12$ .	213
6.16	Solitary wave propagation. Velocity vector distribution at various time levels: (a) $t = 0.0$ ; (b) $t = 2.28$ ; (c) $t = 4.58$ , (d) $t = 6.84$ ; (e) $t = 9.12$ .	214
6.17	Wave heights with respect to time on the right and left side walls: (a) right wall; (b) left wall.	214

6.18	Solitary wave propagation. Comparison of wave heights with experimental data [74].	215
6.19	Natural convection in a square enclosure. Streamlines and isotherms for different Rayleigh numbers. (a) $Ra = 10^4$ ; (b) $Ra = 10^5$ ; (c) $Ra = 10^7$ .	217
6.20	Natural convection in a square enclosure. Adapted meshes for (a) $Ra = 10^5$ and (b) $Ra = 10^6$ .	218
7.1	Boundaries of a computation domain. $\Gamma_u$ , wall boundary; $\Gamma_s$ , fictitious boundary.	228
7.2	Characteristic directions at inlet and exit for supersonic and subsonic flows.	230
7.3	Subsonic inviscid flow past a NACA0012 airfoil at Mach number of 0.25 and zero angle of attack. Smoothed density contours [68].	235
7.4	Subsonic inviscid flow past a NACA0012 airfoil at Mach number of 0.25 and zero angle of attack. Comparison between smoothed and unsmoothed pressure coefficients [68].	235
7.5	The Riemann shock tube problem [1,69]. The total length is divided into 100 elements. Profile illustrated corresponds to 70 time steps ( $\Delta t = 0.25$ ). Lapidus constant $C_{Lap} = 1.0$ .	236
7.6	Isothermal flow through a nozzle [1]. Forty elements of equal size used: (a) subsonic inflow and outflow; (b) supersonic inflow and outflow; (c) supersonic inflow-subsonic outflow with shock.	237
7.7	Transient supersonic flow over a step in a wind tunnel [5] (problem of Woodward and Colella [71]). Inflow Mach 3 uniform flow: (a) structured uniform mesh; (b) solution – contours of pressure at various times.	239
7.8	Inviscid flow past a NACA0012 aerofoil. Unstructured mesh. Number of nodes: 3753; number of elements: 7351. (a) Finite element mesh and domain; (b) mesh distribution in the vicinity of the aerofoil.	240
7.9	Inviscid flow past a NACA0012 aerofoil. Convergence histories to steady state.	241
7.10	Inviscid subsonic flow past a NACA0012 aerofoil. Pressure contours: (a) Mach number = 0.25; (b) Mach number = 0.5	241
7.11	Inviscid subsonic flow past a NACA0012 aerofoil. Pressure coefficient distribution: (a) Mach number = 0.25; (b) Mach number = 0.5	242
7.12	Inviscid transonic and supersonic flow past a NACA0012 aerofoil. Pressure contours: (a) Mach number = 0.85; (b) Mach number = 0.95; (c) Mach number = 1.2.	242
7.13	Inviscid transonic and supersonic flow past a NACA0012 aerofoil. Pressure coefficient distribution: (a) Mach number = 0.85; (b) Mach number = 0.95; (c) Mach number = 1.2.	243

7.14	Mesh enrichment. (a) Triangle subdivision. (b) Restoration of connectivity.	244
7.15	Supersonic, Mach 3, flow past a wedge. Exact solution forms a stationary shock. Successive mesh enrichment and density contours.	245
7.16	Reflection of a shock wave at a wall [11]: Euler equations. A sequence of meshes: (a) nodes: 279, elements: 478; (b) nodes: 265, elements: 479; (c) nodes: 285, elements: 528; and corresponding pressure contours, (d) to (f).	247
7.17	Hypersonic flow past a blunt body [11] at Mach 25, 22° angle of attack. (a) Sequence of meshes deployed; (b) the corresponding density; (c) the corresponding pressure contours. Initial mesh, nodes: 547, elements: 978; first mesh, nodes: 383, elements: 696; final mesh, nodes: 821, elements: 1574.	248
7.18	Supersonic flow past a full cylinder [61]. $M = 3$ : (a) geometry and boundary conditions; (b) adapted mesh, nodes: 12651, elements: 24,979; (c) Mach contours using second derivative shock capture; (d) Mach contours using anisotropic shock capture.	249
7.19	Supersonic flow past a full cylinder [61]. $M = 3$ : comparison of (a) coefficient of pressure, (b) Mach number distribution along the mid-height and cylinder surface.	250
7.20	Interaction of an impinging and bow shock wave [77]. Adapted mesh and pressure contours.	251
7.21	Inviscid flow past an ONERA M6 wing. Density contours. Mach number = 0.78, angle of attack to horizontal = 2.8°.	253
7.22	Adaptive three-dimensional solution of compressible inviscid flow around a high-speed (Mach 2) aircraft [84]. Nodes: 70,000, elements: 125,000.	254
7.23	Three-dimensional analysis of an engine intake [84] at Mach 2 (14,000 elements): (a) mesh on analysis surface; (b) mesh on analysis surface; (c) pressure contours.	255
7.24	Supersonic car, THRUST SSC [35]. (a) car and (b) finite element surface mesh. ( <i>Image used in (a) courtesy of SSC Programme Ltd. Photographer Jeremy C.R. Davey.</i> )	257
7.25	Supersonic car, THRUST SSC [35] pressure contours: (a) full configuration; (b) front portion.	258
7.26	Supersonic car, THRUST SSC [35] comparison of finite element and experimental results.	258
7.27	A transient problem with adaptive remeshing [88]. Simulation of a sudden failure of a pressure vessel. Progression of refinement and velocity patterns shown. Initial mesh 518 nodes.	259
7.28	A transient problem with adaptive remeshing [88]. Model of the separation of shuttle and rocket. Mach 2, angle of attack $-4^\circ$ , initial mesh 4130 nodes.	260

7.29	Separation of a generic shuttle vehicle and rocket booster [32]. (a) Initial surface mesh and surface pressure; (b) final surface mesh and surface pressure.	261
7.30	Refinement in the boundary layer: (a) a two-dimensional sub-layer of structured quadrilaterals; (b) a three-dimensional sub-layer of prismatic elements.	261
7.31	Viscous flow past a flat plate (Carter problem) [92]. Mach 3, $Re = 1000$ . (a) Mesh, nodes: 6750, elements: 13,172. Contours of (b) pressure and (c) Mach number.	263
7.32	Viscous flow past a flat plate (Carter problem) [92]. Mach 3, $Re = 1000$ . (a) Pressure distribution along the plate surface, (b) exit velocity profile.	264
7.33	Shock and boundary layer interaction [94]. Final mesh, nodes: 4198. (a) Initial and final (second) adapted mesh; (b) initial and final (second) pressure contours; (c) initial and final (second) Mach number contours; (d) surface pressure and skin tension.	265
7.34	Hybrid mesh for supersonic viscous flow past a NACA0012 aerofoil [95], Mach 2, and contours of Mach number: (a) initial mesh; (b) first adapted mesh; (c) final mesh; (d) mesh near stagnation point (shown opposite).	268
7.35	Structured grid in boundary layer for a two-component aerofoil [25]. Advancing boundary normals.	269
7.36	Transonic viscous flow past a NACA0012 aerofoil. Mach number 0.85, Reynolds number = 2000. (a) Finite element mesh; (b) structured layers close to the wall.	270
7.37	Transonic viscous flow past a NACA0012 aerofoil. Mach number 0.85, Reynolds number = 2000. Mach contours.	270
7.38	Transonic viscous flow past a NACA0012 aerofoil. Mach number 0.85, Reynolds number = 2000. (a) surface pressure and (b) friction coefficients distribution.	271
7.39	Hypersonic viscous flow past a double ellipsoid. Unstructured mesh with structured mesh layers close to the walls: (a) adapted mesh; (b) structured layers close to the wall; (c) close-up of structured layers.	272
7.40	Hypersonic viscous flow past a double ellipsoid. Density contours.	272
8.1	Random variation of velocity in a turbulent flow with respect to time.	284
8.2	(a) Structured mesh S1 (nodes: 15,625; elements: 69,120); (b) unstructured mesh U1 (nodes: 23,597; elements: 127,692).	292

8.3	Wall distance contours at a central section in the $x_1$ direction (uniformly structured mesh S1). Comparison between search procedure and implicit GMRES scheme. (a) Simple search procedure (structured mesh): $\phi_{min} = 0.0, \phi_{max} = 0.5000$ ; (b) Eikonal equation (structured mesh): $\phi_{min} = 0.0, \phi_{max} = 0.5000$ ; (c) simple search procedure (unstructured mesh): $\phi_{min} = 0.0, \phi_{max} = 0.4923$ ; (d) Eikonal equation (unstructured mesh): $\phi_{min} = 0.0, \phi_{max} = 0.4887$ .	293
8.4	Turbulent incompressible flow through a rectangular channel using the Spalart-Allmaras model at $Re = 12,300$ . Logarithmic representation of time-averaged velocity profile. (Note: $u^+ = u/u_\tau$ with $u_\tau = \sqrt{\tau_w/\rho}$ being the friction velocity; $y^+ = yu_\tau/\nu$ with $y$ being the shortest distance to the wall.)	294
8.5	Turbulent incompressible flow in a rectangular channel using the Spalart-Allmaras model at $Re = 12,300$ . (a) Comparison of fully developed velocity profiles; (b) convergence to the steady state.	295
8.6	Turbulent flow past a two-dimensional backward facing step. Problem definition.	296
8.7	Incompressible turbulent flow past a backward facing step. Velocity profiles at various downstream sections at $Re = 3025$ : (a) one-equation model; (b) SA model; (c) two-equation model.	297
8.8	Incompressible turbulent flow past a backward facing step. (a) Structured mesh (elements: 8092, nodes: 4183), (b) velocity contours, (c) $\hat{v}$ contours, and (d) pressure contours at $Re = 3015$ using the SA model.	298
8.9	Incompressible turbulent flow past a backward facing step. (a) Unstructured mesh (elements: 47,359, nodes: 24,336), (b) velocity contours, and (c) $\hat{v}$ contours at $Re = 3025$ using the SA model.	299
8.10	Incompressible turbulent flow past a circular cylinder. Finite element mesh: (a) overall mesh; (b) close-up of the cylinder.	300
8.11	Incompressible turbulent flow past a circular cylinder. Snapshots of variables at $Re = 10,000$ using the SA model: (a) $u_1$ contours; (b) $p$ contours; (c) $v_T$ contours.	301
8.12	Incompressible turbulent flow past a circular cylinder. (a) Drag and (b) lift coefficient distributions with respect to real time at $Re = 10,000$ using the SA model.	302
8.13	Incompressible turbulent flow past a circular cylinder. Time-averaged coefficient of pressure at $Re = 10,000$ using the SA model. Data for comparison from Ref. [20].	303
9.1	Typical examples of porous media.	310
9.2	Fluid saturated porous medium. Infinitesimal control volume.	311
9.3	Forced convection in a channel filled with a variable porosity medium. Geometry and boundary conditions.	317



9.4	Forced convection in a channel. Comparison of Nusselt number with experimental data for different particle Reynolds numbers. Points—experimental [24]; dashed line—numerical [24]; solid line—CBS.	318
9.5	Forced convection in a channel. Comparison between the generalized model and the Forcheimner and Brinkman extensions to Darcy's law.	319
9.6	Natural convection in a fluid-saturated variable-porosity medium. Problem boundary conditions.	320
9.7	Buoyancy driven flow in a fluid-saturated porous medium. Finite element mesh (nodes: 2601, elements: 5000).	321
9.8	Natural convection in a fluid-saturated porous, square enclosure. Vector plots and temperature contours for different Rayleigh and Darcy numbers, $Pr = 0.71$ .	322
9.9	Natural convection in a fluid-saturated constant-porosity medium. Problem definition.	323
9.10	Natural convection in a fluid-saturated constant-porosity medium within an annular enclosure. Comparison of hot wall steady-state Nusselt number with the experimental and numerical data [32].	324
10.1	The shallow-water problem. Notation: (a) coordinates; (b) velocity distribution.	328
10.2	Shoaling of a wave: (a) problem statement; (b) solution, for 40, 80, and 160 elements at various times.	335
10.3	Propagation of waves due to dam break ( $C_{Lap} = 0$ ). Forty elements in analysis domain. $C = \sqrt{gH} = 1$ , $\Delta t = 0.25$ .	336
10.4	A "bore" created in a stream due to water level rise downstream (A). Level at A, $\eta = 1 - \cos \pi t/30$ ( $0 \leq t \leq 30$ ), $2$ ( $30 \leq t$ ). Levels and velocities at intervals of 5 time units, $\Delta t = 0.5$ .	337
10.5	Steady-state oscillation in a rectangular channel due to periodic forcing of surface elevation at an inlet. Linear frictional dissipation [32].	338
10.6	Location map. Bristol Channel and Severn Estuary.	339
10.7	Finite element meshes. Bristol Channel and Severn Estuary.	340
10.8	Velocity vector plots (FL mesh).	341
10.9	Finite element mesh used in the Severn bore calculations (a) Full domain (b) Part of the domain between points A and B (c) Part of the domain beyond point B.	342
10.10	Severn tsunامي. Generation during high tide. Water height contours (times after generation).	344
10.11	Wave-induced steady-state flow past a harbor [30].	345
10.12	Supercritical flow and formation of shock waves in symmetric channel of variable width contours of $h$ . Inflow Froude number $= 2.5$ . Constriction: $15^\circ$ .	345
10.13	Adjustment of boundary due to tidal variation.	346